

Analytical computation of the optimal reference currents for MTPC/MTPA, MTPV and MTPF operation of anisotropic synchronous machines considering stator resistance and mutual inductance

Christoph M. Hackl*, Julian Kullick, Hisham Eldeeb and Lorenz Horlbeck
Technical University of Munich (TUM)

Lichtenbergstr. 4a

Garching, Germany

Phone*: +49 (89) 289-52725

Fax: +49 (89) 289-52799

Email*: christoph.hackl@tum.de

URL: <http://www.cres.mse.tum.de>

Acknowledgments

This project has received funding from the European Union's Horizon ITN2020 research and innovation programme under the Marie Skłodowska-Curie grant agreement No. 642682, and from the Bavarian Ministry for Education, Culture, Science and Art.

Keywords

«Efficiency», «Electrical drive», «Mechatronics», «Optimal control», «Ohmic losses», «Maximum-Torque-per-Ampere/Current (MTPA/MTPC)», «Maximum-Torque-per-Flux (MTPF)», «Maximum-Torque-per-Voltage (MTPV)»

Abstract

The derivation of analytical solutions for the optimal reference currents during Maximum-Torque-per-Current (MTPC; or Maximum-Torque-per-Ampere (MTPA)), Maximum-Torque-per-Voltage (MTPV) and Maximum-Torque-per-Flux (MTPF) operation of anisotropic synchronous machines with *non-negligible* stator resistance and mutual inductance is presented. The analytical solutions allow for a direct computation of the corresponding reference currents without neglecting stator resistance and/or mutual inductance (as usually done). Numerical approximations are *no longer* required. The derived analytical solutions for MTPC, MTPV and MTPF operation are suitable for any anisotropic synchronous machine; even for nonlinear reluctance synchronous machines as measurement will illustrate.

Introduction and motivation

Electrical machines consume more than half of the globally generated electricity [1]. Hence, optimal feedforward torque control of electric drives (machine+inverter) is crucial to minimize losses; in particular for synchronous machines (SMs) with non-negligible anisotropy such as *interior permanent-magnet (PM) synchronous motors (IPMSMs)*, *reluctance synchronous machines (RSMs)*, *PM-assisted RSMs (PMA-RSMs)* or *PM-enhanced RSMs (PME-RSMs)* [2, 3]. The optimal feedforward torque control problem was discussed in numerous publications, see e.g. [4, 5, 6, 7, 8] to name a few. The computation of the optimal reference currents for the different operation strategies such as MTPC, MTPV or MTPF is usually done either *numerically* or *analytically imposing simplifying assumptions* (e.g. *neglecting stator resistance and/or cross-coupling inductance*) on machine model or physical constraints. Numerical solutions, in general, increase the computational load on the real-time system. Analytical solutions are more

attractive (easy to implement, more accurate and faster to compute). However, to the best knowledge of the authors, analytical solutions *which simultaneously consider* stator resistance *and* mutual inductance for MTPC, MTPV and MTPF of anisotropic SMs are *not* available yet. In [9, Sec. IV] and [10, Sec. 2.2.3], it was stated that the derivation of a general analytical solution of the optimal currents for MTPC, MTPV and MTPF *considering* stator resistance *and* mutual inductance seems *not possible* due to the mathematical complexity. The main contributions of this paper are: (i) The derivation of analytical solutions of the optimal reference currents for MTPC, MTPV and MTPF operation explicitly *considering stator resistance and cross-coupling (mutual) inductance*. The proposed analytical solutions ensure (i-a) definite convergence to the optimal reference currents (compared to numerical methods), (i-b) simple implementation, and (i-c) reduced computational load; (ii) The analytical solutions for the optimal reference currents are obtained by (ii-a) the use of *Lagrangian multipliers* and (ii-b) an *implicit* problem formulation as *quadrics* (i.e. all constraints and operation strategies—such as e.g. current circle, voltage ellipse and torque hyperbola—are reformulated implicitly in the (d, q) -plane as quadric surfaces); (iii) The impact of neglecting stator resistance and mutual inductance or both on the optimality of all operation strategies is illustrated showing that neglecting these two parameters during optimization yields deviations between optimal and approximated reference currents; and (iv) Simulation and experimental results confirm the theoretical outcomes.

Problem formulation

Main goal of optimal feedforward torque control is to obtain the optimal reference currents for a given reference torque considering the actual operation mode of the electrical drive system and its physical constraints. To do so, at first, the steady-state model and the operation constraints of the considered synchronous machines, and the problem formulation are presented. Then, the machine torque and all operation constraints (such as current or voltage limit) are re-formulated *implicitly* as *quadratic surfaces (quadrics)*. These implicit expressions will allow for an analytical computation of the reference currents for MTPC, MTPV or MTPF operation.

Steady-state model of generic synchronous machines (SMs)

The steady-state model of an anisotropic synchronous machine in the $k = (d, q)$ -reference frame¹ (matrix/vector notation) is given by

$$\boxed{u_s^k = R_s i_s^k + \omega_k J L_s^k i_s^k + \omega_k J \psi_{pm}^k}, \quad (1)$$

where $J := \begin{bmatrix} 0 & -1 \\ 1 & 0 \end{bmatrix}$ and a (locally) *constant* inductance matrix $L_s^k \in \mathbb{R}^{2 \times 2}$ (e.g. obtained by linearizing the nonlinear flux linkage at the actual operating point) is assumed such that the (local approximation of the) flux linkage may be expressed by

$$\psi_s^k(i_s^k) = L_s^k i_s^k + \psi_{pm}^k \quad \text{where} \quad \psi_{pm}^k = \begin{pmatrix} \psi_{pm}^d \\ \psi_{pm}^q \end{pmatrix} = \begin{cases} (\psi_{pm}, 0)^\top, & \text{for PMSM and PME-RSM [3],} \\ (0, -\psi_{pm})^\top, & \text{for PMA-RSM [3, 2], and} \\ (0, 0)^\top, & \text{for RSM [3, 13].} \end{cases} \quad (2)$$

The machine torque is then given by

$$m_m(i_s^k) \stackrel{(2)}{=} \frac{3}{2} n_p \left[(i_s^k)^\top J L_s^k i_s^k + (i_s^k)^\top J \psi_{pm}^k \right] = \frac{3}{2} n_p \left[\psi_{pm}^d i_s^q - \psi_{pm}^q i_s^d + (L_s^d - L_s^q) i_s^d i_s^q + L_m ((i_s^d)^2 - (i_s^q)^2) \right]. \quad (3)$$

In (1), (2) and (3), R_s (in Ω) is the stator resistance, $u_s^k := (u_s^d, u_s^q)^\top$ (in V), $i_s^k := (i_s^d, i_s^q)^\top$ (in A) and $\psi_s^k := (\psi_s^d, \psi_s^q)^\top$ (in Wb) are stator voltage, current and flux linkage vectors, respectively. Note that $\omega_k = n_p \omega_m$ (in rad/s) is the *electric* angular frequency, whereas ω_m is the *mechanical* angular frequency of the machine. n_p is the pole pair number. The inductance matrix $L_s^k = (L_s^k)^\top := \begin{bmatrix} L_s^d & L_m^q \\ L_m^d & L_s^q \end{bmatrix} > 0$ depends

¹I.e., the synchronously rotating $k = (d, q)$ -coordinate system with orthogonal axes d and q after Clarke and Park transformation (see [11] or [12, Chapt. 14] with identical notation as in this paper).

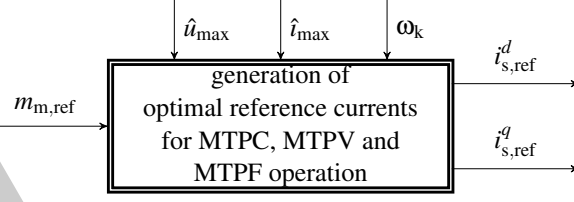


Fig. 1: Optimal reference currents $i_s^k = (i_{s,\text{ref}}^d, i_{s,\text{ref}}^q)^\top$ for given reference torque $m_{m,\text{ref}}$ and actual angular velocity $\omega_k = n_p \omega_m$, and current \hat{i}_{max} and voltage \hat{u}_{max} constraints.

on stator inductances $L_s^q > 0$, $L_s^d > 0$ (both in H) and cross-coupling (mutual) inductance² $L_m \in \mathbb{R}$ (in H) satisfying $L_s^d L_s^q - L_m^2 > 0$. The permanent-magnet flux linkage is denoted by $\Psi_{\text{pm}}^k = (\Psi_{\text{pm}}^d, \Psi_{\text{pm}}^q)^\top$.

Remark 1 (Affine flux linkage) Eq. (2) implies a constant inductance matrix; this is in line with most of the recent publications which deal also with constant inductances only (see e.g. [6, 7]). This simplification is not true in general [13]. The results of this paper can be considered as a generalization of the results for IPMSM in [5] to any anisotropic SM (e.g. PMA/PME-RSMs and RSMs) with non-negligible stator resistance R_s and mutual inductance L_m . Moreover, measurement results presented later will illustrate applicability to nonlinear machines (with current-dependent differential inductances) as well.

Operation constraints and problem formulation

Stator current and voltage vectors must not exceed their respective maximal magnitudes $\hat{i}_{\text{max}} > 0$ (in A) and $\hat{u}_{\text{max}} > 0$ (in V; both are amplitudes *not* RMS values here), i.e.

$$\|i_s^k\|^2 = (i_s^d)^2 + (i_s^q)^2 \leq \hat{i}_{\text{max}}^2 \quad \text{and} \quad \|u_s^k\|^2 = (u_s^d)^2 + (u_s^q)^2 \leq \hat{u}_{\text{max}}^2. \quad (4)$$

For a given reference torque $m_{m,\text{ref}}$ (in Nm), the general objective is to find optimal and analytical solutions of the reference currents for the MTPC, MTPV and MTPF operation. Hence, the following optimization problem

$$\max_{i_s^k} -f(i_s^k) \quad \text{s.t.} \quad \|u_s^k\| \leq \hat{u}_{\text{max}}, \|i_s^k\| \leq \hat{i}_{\text{max}}, |m_m(i_s^k)| \leq |m_{m,\text{ref}}| \quad \text{and} \quad \text{sign}(m_{m,\text{ref}}) = \text{sign}(m_m(i_s^k)), \quad (5)$$

with three inequality constraints and one equality constraint must be solved online, where obviously the sign of reference and machine torque should coincide. The function $f(i_s^k)$ depends on the operation strategy (e.g. $f(i_s^k) = \|i_s^k\|^2$ for MTPC). The most favorable outcome is an analytical solution of the optimal reference current vector

$$i_{s,\text{ref}}^k(m_{m,\text{ref}}, \hat{u}_{\text{max}}, \hat{i}_{\text{max}}, \omega_k) = \begin{pmatrix} i_{s,\text{ref}}^d(m_{m,\text{ref}}, \hat{u}_{\text{max}}, \hat{i}_{\text{max}}, \omega_k) \\ i_{s,\text{ref}}^q(m_{m,\text{ref}}, \hat{u}_{\text{max}}, \hat{i}_{\text{max}}, \omega_k) \end{pmatrix} := \arg \max_{i_s^k} -f(i_s^k), \quad (6)$$

which is then handed over to any underlying current controller (see also Fig. 1).

Remark 2 (Feasible reference torques and non-convexity of the machine torque) Due to the voltage limit or due to the current limit, not all reference torques $m_{m,\text{ref}}$ are feasible during all operation modes. Therefore, the additional inequality constraint in (5) is considered. If the requested reference torque is feasible, the inequality constraint becomes the equality constraint $|m_m(i_s^k)| = |m_{m,\text{ref}}|$ (or simply, $m_m(i_s^k) = m_{m,\text{ref}}$). Moreover, note that the machine torque $m_m(i_s^k) \propto (i_s^k)^\top J L_s^k i_s^k$ is not convex, since $J L_s^k = \begin{bmatrix} -L_m & -L_s^q \\ L_s^d & L_m \end{bmatrix}$ is non-symmetric and indefinite with eigenvalues $\pm \sqrt{L_m^2 - L_s^d L_s^q}$. Hence, maximizing the machine torque is not in general a viable approach.

²Note that the mutual inductance L_m changes its sign with the negative product of the currents, i.e. $\text{sign}(L_m) = -\text{sign}(i_s^d \cdot i_s^q)$ [14, Fig. 2].

Implicit reformulation of machine torque and constraints (as quadrics)

The basis for the upcoming derivations is the steady-state model in (1). The non-intuitive trick to derive analytical solutions for the reference currents for MTPC, MTPV or MTPF operation is the re-formulation of the general optimization problem (5) *implicitly by quadrics (or quadric surfaces)* which allows to invoke the Lagrangian formalism (without the need of case studies). In the next sub-sections, the implicit forms of torque hyperbola, voltage ellipse (elliptical area), current circle (circular area) and flux norm are presented. Stator resistance $R_s \neq 0$ and mutual inductance $L_m \neq 0$ will *not* be neglected to present the most general result.

Reference torque hyperbola (constant reference torque trajectory)

To derive the quadric of the torque hyperbola, define the following matrix, vector and scalar

$$T := \frac{3}{4}n_p(JL_s^k + L_s^kJ^\top) = \frac{3}{2}n_p \begin{bmatrix} -L_m & \frac{L_s^d - L_s^q}{2} \\ \frac{L_s^d - L_s^q}{2} & L_m \end{bmatrix} = T^\top, \quad t := \frac{3}{4}n_p J\psi_{pm}^k \quad \text{and} \quad \tau(m_{m,\text{ref}}) := -m_{m,\text{ref}}, \quad (7)$$

respectively. Moreover, observe that $(i_s^k)^\top JL_s^k i_s^k = (i_s^k)^\top L_s^k J^\top i_s^k$, therefore $\frac{3}{4}n_p (i_s^k)^\top (JL_s^k + L_s^kJ^\top) i_s^k = (i_s^k)^\top T i_s^k$. Then, by combining (7) and the relations above with (3), the machine torque can be expressed by $m_m(i_s^k) = (i_s^k)^\top T i_s^k + 2t^\top i_s^k$; which, for a given reference torque $m_{m,\text{ref}}$ and (7), yields the *machine reference torque hyperbola* (a quadric) as follows

$$\mathbb{T}(m_{m,\text{ref}}) := \{ i_s^k \in \mathbb{R}^2 \mid (i_s^k)^\top T i_s^k + 2t^\top i_s^k + \tau(m_{m,\text{ref}}) = 0 \}. \quad (8)$$

An exemplary torque hyperbola is plotted in Fig. 2 (see black line — in Fig. 2).

Voltage elliptical area (reformulation of the voltage constraint in (4))

Inserting (1) into (4) and squaring the result yields an expression of the voltage limit in (4) which can be stated implicitly as quadric surface $\mathbb{V}(\omega_k, \hat{u}_{\text{max}}) := \{ i_s^k \in \mathbb{R}^2 \mid (i_s^k)^\top V(\omega_k) i_s^k + 2v(\omega_k)^\top i_s^k + v(\omega_k, \hat{u}_{\text{max}}) \leq 0 \}$, where respective matrix, vector and scalar are given by [16]

$$\left. \begin{aligned} V(\omega_k) &:= R_s^2 I_2 + R_s \omega_k (JL_s^k + L_s^kJ^\top) + \omega_k^2 (L_s^k)^2 = V(\omega_k)^\top \\ &= \begin{bmatrix} R_s^2 - 2\omega_k R_s L_m + \omega_k^2 [(L_s^d)^2 + L_m^2], & \omega_k R_s (L_s^d - L_s^q) + \omega_k^2 L_m (L_s^d + L_s^q) \\ \omega_k R_s (L_s^d - L_s^q) + \omega_k^2 L_m (L_s^d + L_s^q), & R_s^2 + 2\omega_k R_s L_m + \omega_k^2 [(L_s^q)^2 + L_m^2] \end{bmatrix}, \\ v(\omega_k)^\top &:= \omega_k (\psi_{pm}^k)^\top (\omega_k L_s^k + R_s J^\top) \quad \text{and} \quad v(\omega_k, \hat{u}_{\text{max}}) := \omega_k^2 (\psi_{pm}^k)^\top J^\top J \psi_{pm}^k - \hat{u}_{\text{max}}^2. \end{aligned} \right\} \quad (9)$$

$\mathbb{V}(\omega_k, \hat{u}_{\text{max}})$ describes the *voltage elliptical area*. Its boundary/the *voltage ellipse* (see green line — in Fig. 2), is defined by

$$\partial\mathbb{V}(\omega_k, \hat{u}_{\text{max}}) := \{ i_s^k \in \mathbb{R}^2 \mid (i_s^k)^\top V(\omega_k) i_s^k + 2v(\omega_k)^\top i_s^k + v(\omega_k, \hat{u}_{\text{max}}) = 0 \}. \quad (10)$$

Since $V(\omega_k)$, $v(\omega_k)$ and $v(\omega_k, \hat{u}_{\text{max}})$ explicitly depend on the electric angular velocity ω_k , the voltage ellipse depends on ω_k , and, hence, it moves in the current locus for varying angular velocities (see Fig. 2).

Current circular area (reformulation of the current constraint in (4))

The current constraint in (4) can also be expressed implicitly as quadric by $\mathbb{I}(\hat{i}_{\text{max}}) := \{ i_s^k \in \mathbb{R}^2 \mid (i_s^k)^\top I_2 i_s^k - \hat{i}_{\text{max}}^2 \leq 0 \}$, which describes the admissible *maximum current circular area*: The magnitude of the stator current vector must not exceed the current limit \hat{i}_{max} . The *maximum current circle* (see orange line — in Fig. 2), i.e. the boundary of $\mathbb{I}(\hat{i}_{\text{max}})$, is defined by $\partial\mathbb{I}(\hat{i}_{\text{max}}) := \{ i_s^k \in \mathbb{R}^2 \mid (i_s^k)^\top I_2 i_s^k - \hat{i}_{\text{max}}^2 = 0 \}$.

Norm of the flux linkage

To operate the machine in MTPF mode, the squared norm of the flux linkage is minimized. The flux norm can also be expressed as quadric as follows $\|\psi_s^k\|^2 \stackrel{(2)}{=} (L_s^k i_s^k + \psi_{pm}^k)^\top (L_s^k i_s^k + \psi_{pm}^k) =: (i_s^k)^\top F i_s^k + 2f^\top i_s^k + \phi$,

where corresponding matrix, vector and scalar are defined by [16]

$$F := (L_s^k)^2 = \begin{bmatrix} (L_s^d)^2 + L_m^2 & L_m(L_s^d + L_s^q) \\ L_m(L_s^d + L_s^q) & (L_s^q)^2 + L_m^2 \end{bmatrix} = F^\top, \quad f := L_s^k \psi_{\text{pm}}^k, \quad \text{and} \quad \phi := \psi_{\text{pm}}^2. \quad (11)$$

Operation strategies

In this section, MTPC, MTPV and MTPF operation are discussed and the analytical solutions for the respective reference currents are presented. A detailed derivation of the presented results is presented in [16]. A description of the overall operation management also covering *field weakening (FW)* and *maximum current (MC)* control can be found in [15].

Maximum-Torque-per-Current (MTPC) hyperbola (considering L_m)

For low speeds, the voltage constraint in (4) is *not* critical. The minimization of copper losses dominates the operation of the machine and the MTPC strategy must be used. The MTPC optimization problem is formulated as follows

$$\max_{i_s^k \in \mathbb{S}} -\|i_s^k\|^2 \quad \text{s.t.} \quad m_m(i_s^k) = (i_s^k)^\top T i_s^k + 2t^\top (i_s^k) \stackrel{!}{=} m_{m,\text{ref}} \stackrel{(7)}{=} -\tau(m_{m,\text{ref}}) \quad (12)$$

with the admissible current set $\mathbb{S} := \mathbb{V}(\omega_k, \hat{u}_{\text{max}}) \cap \mathbb{I}(\hat{i}_{\text{max}})$ which is the intersection of voltage elliptical area $\mathbb{V}(\omega_k, \hat{u}_{\text{max}})$ and current circular area $\mathbb{I}(\hat{i}_{\text{max}})$. Its solution, the MTPC hyperbola (see blue line — in Fig. 2), can also be expressed implicitly as quadric [16]

$$\text{MTPC} := \{ i_s^k \in \mathbb{R}^2 \mid (i_s^k)^\top M_C i_s^k + 2m_C^\top i_s^k = 0 \}. \quad (13)$$

The derivation of the implicit form (13) and the explicit expressions for M_C and m_C are presented in Appendix B of [16]. Note that the derivation in Appendix B of [16] can also be applied to obtain the implicit forms of the two other operation strategies such as MTPV or MTPF. Due to space limitations, a detailed derivation cannot be presented in this paper.

Maximum-Torque-per-Voltage (MTPV) hyperbola (considering R_s and L_m)

For high speeds, the voltage constraint in (4) is critical and dominates the operation of the machine. Now, the operation strategy is MTPV. The corresponding MTPV optimization problem is as follows

$$\max_{i_s^k \in \mathbb{S}} -\|u_s^k(i_s^k)\|^2 \quad \text{s.t.} \quad m_m(i_s^k) = (i_s^k)^\top T i_s^k + 2t^\top (i_s^k) \stackrel{!}{=} m_{m,\text{ref}} \quad (14)$$

with admissible set $\mathbb{S} = \mathbb{V}(\omega_k, \hat{u}_{\text{max}}) \cap \mathbb{I}(\hat{i}_{\text{max}})$. Its solution, the MTPV hyperbola, depends on ω_k and is implicitly given by the quadric [16]

$$\text{MTPV}(\omega_k) := \{ i_s^k \in \mathbb{R}^2 \mid (i_s^k)^\top M_V(\omega_k) i_s^k + 2m_V(\omega_k)^\top i_s^k + \mu_V(\omega_k) = 0 \} \quad (15)$$

Details of the derivation of (15) and the explicit expressions for M_V , m_V and μ_V can again be found in [16]. Note that, due to its dependency on ω_k , the MTPV hyperbola is moving in the (i_s^d, i_s^q) -plane for varying speeds (see light blue line — in Fig. 2).

Maximum-Torque-per-Flux (MTPF) hyperbola (considering L_m)

An alternative to the MTPV strategy is the MTPF strategy. Nevertheless, it should be noted that MTPV should be used, since it yields larger reference currents than those obtained from MTPF (see Remark IV.6 in [16]). The MTPF optimization problem is formulated as follows

$$\max_{i_s^k \in \mathbb{S}} -\|\psi_s^k(i_s^k)\|^2 \quad \text{s.t.} \quad m_m(i_s^k) = (i_s^k)^\top T i_s^k + 2t^\top (i_s^k) \stackrel{!}{=} m_{m,\text{ref}} \quad (16)$$

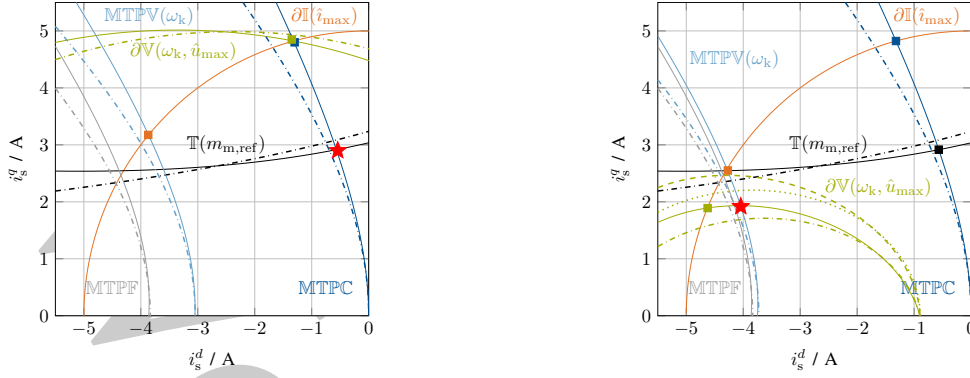


Fig. 2: Steady-state simulation results and illustration of impact of neglecting stator resistance (dashed line: $R_s = 0$), mutual inductance (dash-dotted: $L_m = 0$) or both (dotted: $R_s = L_m = 0$) on e.g. MTPC and MTPV operation: The plots show voltage ellipse $\partial V(\omega_k, \hat{u}_{\max})$, $\partial V(\omega_k, \hat{u}_{\max}; R_s = 0)$, $\partial V(\omega_k, \hat{u}_{\max}; L_m = 0)$, $\partial V(\omega_k, \hat{u}_{\max}; R_s = L_m = 0)$, max. current circle $\partial \mathbb{I}(\hat{i}_{\max})$, MTPC hyperbola MTPC , $\text{MTPC}(L_m = 0)$, reference torque hyperbola $\text{T}(m_{m,\text{ref}})$, $\text{T}(m_{m,\text{ref}}; L_m = 0)$, MTPV hyperbola $\text{MTPV}(\omega_k)$, $\text{MTPV}(\omega_k; L_m = 0)$, MTPF hyperbola MTPF , $\text{MTPF}(L_m = 0)$ and optimal operation point \star .

with admissible set $\mathbb{S} := \mathbb{V}(\omega_k, \hat{u}_{\max}) \cap \mathbb{I}(\hat{i}_{\max})$. Its solution, the MTPF hyperbola (see gray line --- in Fig. 2) is implicitly given by the quadric [16]

$$\text{MTPF} := \{ i_s^k \in \mathbb{R}^2 \mid (i_s^k)^\top M_F i_s^k + 2m_F^\top i_s^k + \mu_F = 0 \}, \quad (17)$$

which does *not* depend on the angular velocity ω_k (in contrast to the MTPV hyperbola (15)). The explicit expressions for M_F , m_F and μ_F are derived in [16].

Analytical solutions of the optimal reference current vectors for MTPC, MTPV and MTPF

The analytical expressions for the optimal reference current vectors are finally given by

$$i_{s,\text{ref}}^k = \begin{cases} i_{s,\text{ref}}^{k,\text{MTPC}}(\lambda^*) := -[\lambda^* T - I_2]^{-1} \lambda^* t, & \text{for MTPC} \\ i_{s,\text{ref}}^{k,\text{MTPV}}(\lambda^*) := -[\lambda^* V(\omega_k) - \text{sign}(m_{m,\text{ref}})T]^{-1} (\lambda^* v(\omega_k) - \text{sign}(m_{m,\text{ref}})t), & \text{for MTPV} \\ i_{s,\text{ref}}^{k,\text{MTPF}}(\lambda^*) := -2 \left[\frac{M_F}{\mu_F} - \frac{V(\omega_k)}{v(\omega_k, \hat{u}_{\max})} - \lambda^* J \right]^{-1} \left(\lambda^* \frac{m_F}{\mu_F} - \frac{v(\omega_k)}{v(\omega_k, \hat{u}_{\max})} \right), & \text{for MTPF} \end{cases} \quad (18)$$

where $I_2 := \begin{bmatrix} 1 & 0 \\ 0 & 1 \end{bmatrix}$, $J := \begin{bmatrix} 0 & -1 \\ 1 & 0 \end{bmatrix}$, and T , t , τ , $V(\omega_k)$, $v(\omega_k)$, $v(\omega_k, \hat{u}_{\max})$, M_F and m_F are as in (7), (9) and (17), respectively. Moreover, λ^* is the optimal Lagrangian multiplier which represents one of the (real) roots of a fourth-order polynomial (for details see Appendices A–D in [16]). Note that these four roots can also be computed analytically (see Appendix A.3 in [16]).

Implementation: Simulation and measurement results

In this section, simulation and measurement results are presented to illustrate the effectiveness of the proposed analytical reference current computation for MPTC, MTPV or MPTF operation. For all presented experiments, exact parameter knowledge is assumed³.

Simulation results: Steady-state simulation and illustration of the impact of neglecting R_s and L_m :

In Fig. 2, for a small 400 W IPMSM with the parameters

$$R_s = 20 \Omega, L_s^d = 60 \text{ mH}, L_s^q = 80 \text{ mH}, L_m = 0.5 \text{ mH}, \psi_{\text{pm}} = 0.23 \text{ Wb} \text{ and } n_p = 3, \quad (19)$$

³As for any parameter-dependent or model-based approach, the impact of parameter uncertainties is usually not negligible. But, due to space limitations, parameter uncertainties are not considered in this paper.

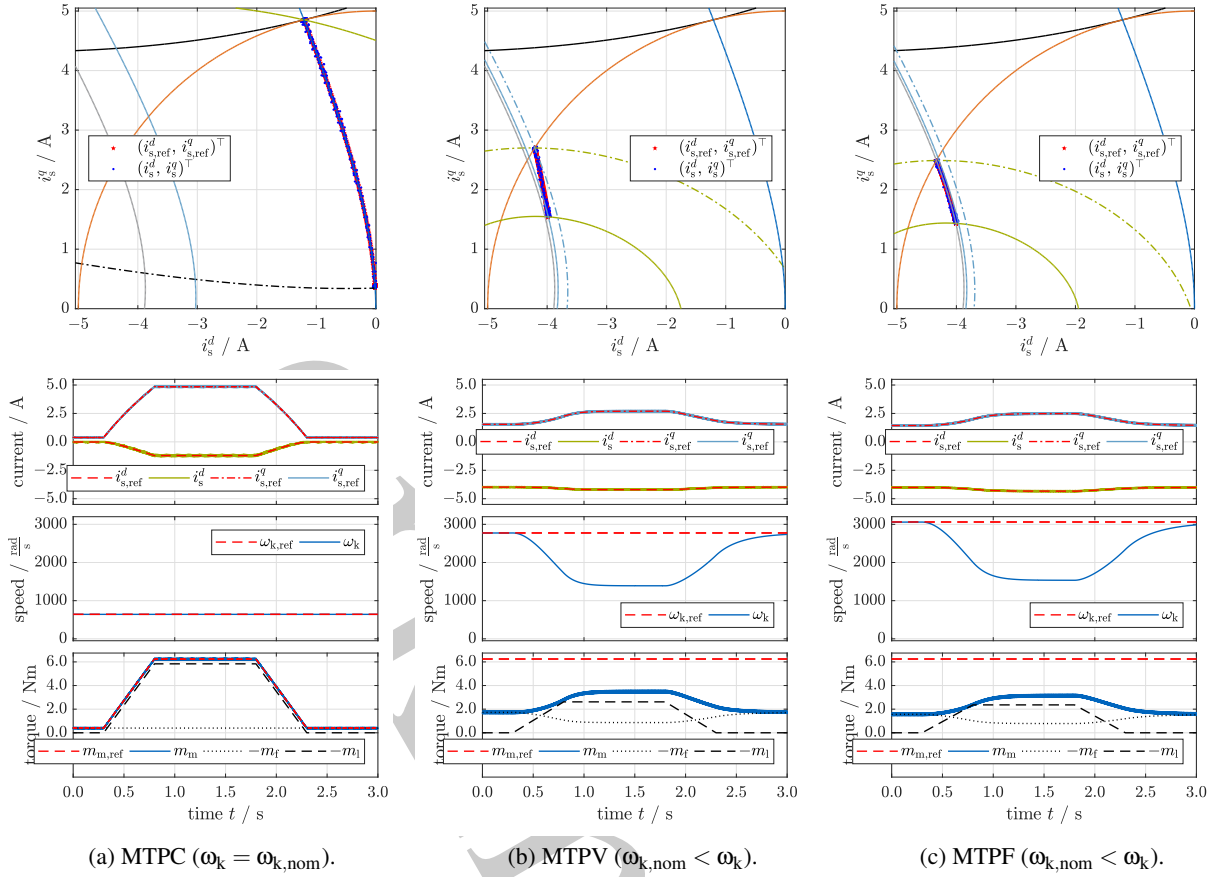


Fig. 3: Current locus (top; signals shown: current circle $\partial\mathbb{I}(\hat{i}_{max})$, reference torque hyperbola(s) $\mathbb{T}(m_{m,ref})$ (& $\mathbb{T}(m_{m,min})$), voltage ellipse(s) $\partial\mathbb{V}(\omega_{k,ref}, \hat{u}_{max})$ (& $\partial\mathbb{V}(\omega_{k,min}, \hat{u}_{max})$), MTFC hyperbola MTFC , MTPV hyperbola(s) $\text{MTPV}(\omega_{k,ref})$ (& $\text{MTPV}(\omega_{k,min})$), MTPF hyperbola MTPF , and optimal reference \star & actual currents \bullet) and corresponding time series plots (bottom; signals shown: reference $i_{s,ref}^d, i_{s,ref}^q$ & actual currents i_s^d, i_s^q , reference $\omega_{k,ref}$ & actual electrical angular velocity ω_k and reference torque $m_{m,ref}$ & actual torque m_m , friction torque m_f and load torque m_l , resp.) for (a) MTFC, (b) MTPV and (c) MTPF.

two different optimal feedforward torque control strategies are illustrated for the positive reference torque $m_{m,ref} = 3.35 \text{ N m}$, the voltage limit $\hat{u}_{max} = 600 \text{ V}$ and the current limit $\hat{i}_{max} = 5 \text{ A}$. The illustrated optimal operation strategies are MTFC in Fig. 2a and MTPV in Fig. 2b. The respective optimal operation points with their (optimal) current references $i_{s,ref}^k = (i_{s,ref}^d, i_{s,ref}^q)^\top$ are indicated by \star and correspond to the intersection of (a) $\text{MTFC} \cap \mathbb{T}(m_{m,ref})$ for MTFC in Fig. 2a and (b) $\text{MTPV} \cap \partial\mathbb{V}(\omega_k, \hat{u}_{max})$ for MTPV in Fig. 2b. For increasing electric angular velocities $\omega_k \in \{1, 3\}\omega_{k,nom}$ (where $\omega_{k,nom} = n_p \omega_{m,nom} = 641.36 \text{ rad s}^{-1}$ is the nominal electric angular velocity), the MTPV hyperbola is approaching the MTPF hyperbola and the voltage ellipse is shrinking; whereas the current circle, MTFC hyperbola, torque hyperbola and MTPF hyperbola are independent of the angular velocity and, hence, do *not* change in the two plots. Moreover, Fig. 2a&b highlight the deteriorating effects on the shape of MTFC, MTPV, MTPF, torque hyperbola and voltage ellipse when (i) stator resistance (i.e. $R_s = 0$: dashed lines), (ii) mutual inductance (i.e. $L_m = 0$: dash-dotted lines) or (iii) both (i.e. $R_s = L_m = 0$: dotted lines) are neglected. Clearly, neglecting stator resistance, mutual inductance or both leads to different (and wrong) intersection points and, hence, *non-optimal* solutions with *reduced efficiency*. Concluding, both parameters should *not* be neglected (at least for machines with low-power rating).

Simulation results: Dynamic simulation of current-controlled IPMSM drive: In Fig. 3 (top: current locus; bottom: time series plots), the dynamic simulation results are shown for MTFC (see Fig. 3a), MTPV (see Fig. 3b) and MTPF (see Fig. 3c) operation of the IPMSM with the parameters as in (19). The implemented dynamical model consists of a PI speed controller and current PI controllers with decou-

pling feedforward control [13], a dynamical model of the IPMSM, and a switching model [12, Chap. 14] of a two-level voltage source inverter (VSI) with space vector modulation (SVM). The switching frequency is $f_{sw} = 10\text{kHz}$. Control objective is tracking of different reference angular velocities $\omega_{k,\text{ref}}$ (if feasible; see --- lines in the third subplots of Fig. 3)). The PI speed controller outputs the reference torque $m_{m,\text{ref}}$ (see --- line in the fourth subplots of Fig. 3) which is fed into the proposed optimal feedforward control system (see Fig. 1). The optimal and analytically computed (with Eq. (18)) reference currents $i_{s,\text{ref}}^d$ and $i_{s,\text{ref}}^q$ (see --- & --- lines in the second subplots and \star in the first subplots of Fig. 3) are then handed over to the current control system. The closed-loop system is subject to a load torque m_l and viscous friction $m_f = v\omega_m$ (with viscous friction coefficient v (in Nm s rad^{-1}); see --- & --- lines in the fourth subplots of Fig. 3, resp.). The closed-loop system responds with the actual currents i_s^d & i_s^q (see --- & --- lines in the second subplots of Fig. 3 and \bullet points in the first subplots of Fig. 3), the actual (feasible) machine torque m_m (see --- line in the fourth subplots of Fig. 3) and the achievable actual electrical angular speed ω_k (see --- line in the third subplots of Fig. 3).

MTPC (see Fig. 3a): Control objective is set-point tracking of the nominal speed, i.e. $\omega_{k,\text{ref}} = \omega_{k,\text{nom}} = 641.36\text{rad s}^{-1}$ under a time-varying load profile where the load torque varies between zero and (almost) nominal torque, i.e. $0 \leq m_l < m_{m,\text{nom}} = 6.24\text{Nm}$. The friction imposes an additional disturbance torque which leads to an overall maximal load of the nominal machine torque. For nominal speed operation, the voltage constraint is not restrictive and MTPC operation is feasible. Hence, all operation points (reference currents) are on the MTPC hyperbola. The current controllers achieve almost perfect tracking of these optimal reference currents. Due to switching in VSI, the actual currents are slightly deteriorated/noisy⁴. All reference torques are feasible and can be applied by the machine. The reference torques $0 \leq m_{m,\text{ref}} \leq m_{m,\text{nom}}$, requested by the speed controller, vary between zero and nominal torque. The desired speed set-point is tracked throughout this experiment.

MTPV (see Fig. 3b): Control objective is speed set-point tracking of $\omega_{k,\text{ref}} = 2773.96\text{rad s}^{-1} \gg \omega_{k,\text{nom}}$ under a time-varying load profile with $0 \leq m_l < 2.3\text{Nm}$. Due to the high speed, the back-emf voltage limits the feasible machine torque. The friction torque at the beginning of the simulation can be compensated for and set-point tracking is achieved. However, when a non-zero additional load torque is applied, the actual machine torque is not sufficient anymore to counteract load and friction. The machine decelerates and the voltage constraints are slightly relaxed (see wider --- voltage ellipse in the current locus) and higher torques can be applied again which stop deceleration but still do not ensure set-point tracking. The reference torque $m_{m,\text{ref}} = m_{m,\text{nom}}$ requested by the speed controller is simply not feasible in MTPV operation. Only at the end of the simulation when the load torque reduces to zero, set-point tracking is feasible again.

MTPF (see Fig. 3c): Control objective is speed set-point tracking of $\omega_{k,\text{ref}} = 3061.20\text{rad s}^{-1} \gg \omega_{k,\text{nom}}$ under a time-varying load profile with $0 \leq m_l < 2.1\text{Nm}$. Similar to MTPV operation, in view of the high speed, the back-emf voltage constraints the machine operation. The feasible torques are reduced to values below 3.1Nm . Again, the friction torque at the beginning of the simulation can be compensated for and set-point tracking is possible. But, when the load torque increases, the produced machine torque is not sufficient. The machine decelerates until the feasible machine torque can counteract load and friction (see wider --- voltage ellipse in the current locus); but speed set-point tracking is not feasible under this overall load. Not before the load torque is reducing to zero again, the reference torque $m_{m,\text{ref}} = m_{m,\text{nom}}$ requested by the speed controller cannot be produced in the machine during MTPF operation. Similarly to the MTPV experiment, at the end of the simulation, set-point tracking is again ensured, since only friction (but no additional load torque) has to be compensated for. Finally, note that, during MTPF operation, reference currents must be tracked with *higher* amplitude than during MTPV operation. Concluding, MTPF operation is *less* efficient than MPTC operation and, hence, MPTV should be the favored operation strategy for high speeds.

Measurement results: The presented theory is also validated by real-time implementation of the proposed analytical MTPC strategy to compute the optimal MTPC reference currents $i_{s,\text{ref}}^k = (i_{s,\text{ref}}^d, i_{s,\text{ref}}^q)^\top$

⁴Increasing the switching frequency would also increase the tracking accuracy of the current control system.

as in (18) for a highly nonlinear custom-built 9.6 kW RSM (Courtesy of Prof. Maarten Kamper, Stellenbosch University, ZA) with the parameters

$$R_s = 0.4 \Omega, \omega_{k,\text{nom}} = 157.07 \text{ rad s}^{-1}, m_{m,\text{nom}} = 61 \text{ N m}, \hat{i}_{\text{max}} = 29.7 \text{ A}, \text{ and } \hat{u}_{\text{max}} = 600 \text{ V}, \quad (20)$$

and the nonlinear (current-dependent) flux linkages ψ_s^d and ψ_s^q and differential inductances L_s^d, L_s^q and L_m as shown in Fig. 4a,b and Fig. 4c,d&e, respectively. The differential inductances are obtained by numerical differentiation of the flux maps with respect to the currents. The overall laboratory setup comprises a dSPACE real-time system, two 22 kW SEW inverters in back-to-back configuration sharing a common DC-link, a HOST-PC running MATLAB/Simulink for rapid-prototyping & data acquisition, the custom-built 9.6 kW RSM and a 14.5 kW SEW PMSM to regulate the mechanical speed. The experiments were conducted for MTPC operation in motor mode (i.e. $\omega_m m_m > 0$) at constant speed $\omega_k \approx \omega_{k,\text{nom}}$. The reference torque $m_{m,\text{ref}}$ was increased step-wise by increments of 1 N m from 0 to 61 N m (nominal torque) and held constant at each step for two seconds. The actual values of the nonlinear flux linkages and inductances were used by the feedforward torque controller at each sampling instant to express the nonlinear RSM dynamics in the form (1) with affine flux linkage (2) by online linearization. The measurement results of analytical and numerical MTPC method were compared. The obtained reference currents of both, the numerical and the analytical torque feedforward controller, are depicted in Fig. 4. Results in Cartesian coordinates and polar coordinates are shown in Fig. 4f and Fig. 4g, respectively. Both methods give almost identical reference currents. The numerical solution yields an unexpected dip around $\|i_s^k\| = 8 \text{ A}$ due to a deteriorated interpolation/accuracy of the numerical solver.

Conclusion

This paper presented analytical expressions for the optimal reference currents during the operation strategies *Maximum-Torque-per-Current (MTPC)* (which, in literature, is often called *Maximum-Torque-per-Ampere (MTPA)*), *Maximum-Torque-per-Voltage (MTPV)* and *Maximum-Torque-per-Flux (MTPF)*, respectively. To the best knowledge of the authors, analytical solutions for the optimal MTPC, MTPV or MTPF current references in particular for anisotropic synchronous machines with *non-negligible* stator resistance and mutual (cross-coupling) inductance were *not* available *this far*.

References

- [1] A. de Almeida, F. Ferreira, and J. Fong, "Ieee industry applications magazine," *Industry Application Magazine*, vol. 17, no. 1, pp. 12–19, 2011.
- [2] I. Boldea, L. Tutelea, Lucian N. Parsa, and D. Dorrell, "Automotive electric propulsion systems with reduced or no permanent magnets: An overview," *IEEE Transactions on Industrial Electronics*, vol. 61, no. 10, pp. 5696–5711, 2014.
- [3] E. Schmidt, "Synchronous reluctance machines with high-anisotropy rotors – comparison of their operational characteristics," in *Proceedings of the Australasian Universities Power Engineering Conference*, pp. 1–6, 2014.
- [4] M. Tursini, E. Chiricozzi, and R. Petrella, "Feedforward flux-weakening control of surface-mounted permanent-magnet synchronous motors accounting for resistive voltage drop," *IEEE Transactions on Industrial Electronics*, vol. 57, no. 11, pp. 440–448, 2010.
- [5] S.-Y. Jung, J. Hong, and K. Nam, "Current minimizing torque control of the IPMSM using Ferrari's method," *IEEE Transactions on Power Electronics*, vol. 28, no. 12, pp. 5603–5617, 2013.
- [6] M. Preindl and S. Bolognani, "Optimal state reference computation with constrained MTPA Criterion for PM motor drives," *IEEE Transactions on Power Electronics*, vol. 30, no. 8, pp. 4524–4535, 2015.
- [7] J. Lemmens, P. Vanassche, and J. Driesen, "PMSM drive current and voltage limiting as a constraint optimal control problem," *IEEE Journal of Emerging and Selected Topics in Power Electronics*, vol. 3, no. 2, pp. 326–338, 2015.
- [8] L. Horlbeck and C. Hackl, "Analytical solution for the MTPV hyperbola including the stator resistance," in *Proceedings of the IEEE International Conference on Industrial Technology (ICIT 2016)*, (Taipei, Taiwan), pp. 1060–1067, 2016.
- [9] R. Ni, D. Xu, G. Wang, L. Ding, G. Zhang, and L. Qu, "Maximum efficiency per ampere control of permanent-magnet synchronous machines," *IEEE Transactions on Industrial Electronics*, vol. 62, no. 4, pp. 2135–2143, 2015.

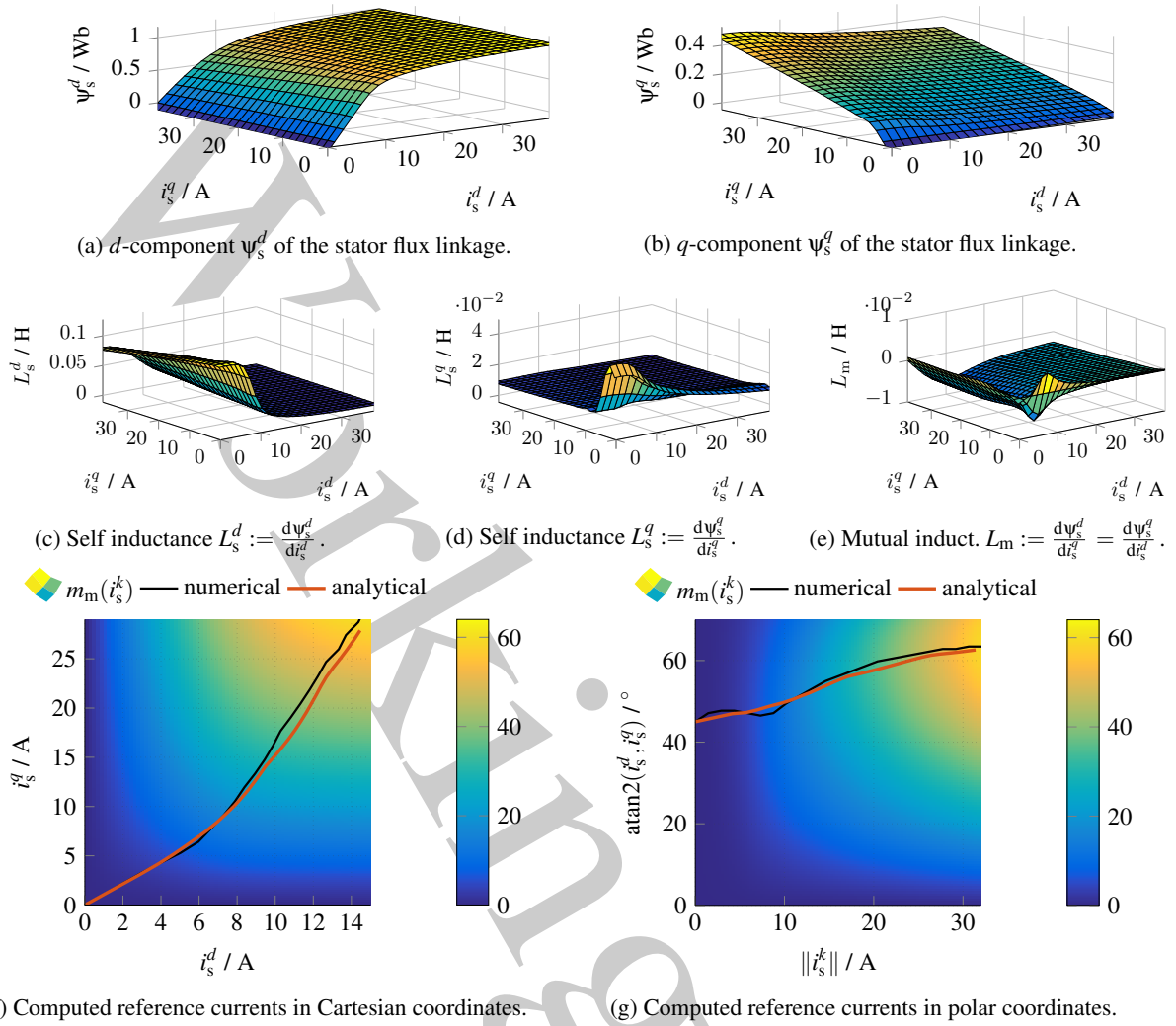


Fig. 4: **Nonlinear flux linkages** (a), (b) and **inductances** (c), (d), (e) of the custom-built 9.6 kW RSM (inductances shown in the first quadrant, i.e. $i_s^d \geq 0$ and $i_s^q \geq 0$) and **measurement results** (f) & (g) at 150rad/s^{-1} : Comparison of the optimal reference currents $i_{s,\text{ref}}^k = (i_{s,\text{ref}}^d, i_{s,\text{ref}}^q)^\top$ for MTPC operation computed by the conventional numerical and the proposed analytical method.

- [10] J. Ahn, S.-B. Lim, K.-C. Kim, J. Lee, J.-H. Choi, S. Kim, and J.-P. Hong, "Field weakening control of synchronous reluctance motor for electric power steering," *IET Electric Power Applications*, vol. 1, no. 4, pp. 565–570, 2007.
- [11] C. Dirscherl, C. Hackl, and K. Schechner, "Modellierung und Regelung von modernen Windkraftanlagen: Eine Einführung," in *Elektrische Antriebe – Regelung von Antriebssystemen* (D. Schröder, ed.), ch. 24, pp. 1540–1614, Springer-Verlag, 2015.
- [12] C. M. Hackl, *Non-identifier based adaptive control in mechatronics: Theory and Application*. No. 466 in Lecture Notes in Control and Information Sciences, Berlin: Springer International Publishing, 2017.
- [13] C. M. Hackl, M. J. Kamper, J. Kullick, and J. Mitchell, "Current control of reluctance synchronous machines with online adjustment of the controller parameters," in *Proceedings of the 2016 IEEE International Symposium on Industrial Electronics (ISIE 2016)*, (Santa Clara, CA, USA), pp. 153–160, 2016.
- [14] C. M. Hackl, M. J. Kamper, J. Kullick, and J. Mitchell, "Nonlinear PI current control of reluctance synchronous machines," *arXiv:1512.09301* (see <https://arxiv.org/pdf/1512.09301>), 2015.
- [15] H. Eldeeb, C. M. Hackl, L. Horlbeck, and J. Kullick, "A unified theory for optimal feedforward torque control of anisotropic synchronous machines," *International Journal of Control*, 2017 (DOI: 10.1080/00207179.2017.1338359).
- [16] H. Eldeeb, C. M. Hackl, L. Horlbeck, and J. Kullick, "On the optimal feedforward torque control problem of anisotropic synchronous machines: Quadratics, quartics and analytical solutions," *arXiv:1611.01629* (see <https://arxiv.org/pdf/1611.01629>), 2016.